HHS Public Access

Author manuscript

ACS Chem Neurosci. Author manuscript; available in PMC 2018 February 15.

Published in final edited form as:

ACS Chem Neurosci. 2017 February 15; 8(2): 272–280. doi:10.1021/acschemneuro.6b00363.

Simultaneous Voltammetric Measurements of Glucose and Dopamine Demonstrate the Coupling of Glucose Availability with Increased Metabolic Demand in the Rat Striatum

Samantha K. Smith, **Christie A. Lee**, **Matthew E. Dausch**, **Brian M. Horman**, **Heather B. Patisaul**, **Gregory S. McCarty**, and **Leslie A. Sombers**

Department of Chemistry, North Carolina State University, Raleigh, North Carolina 27695-8204

Abstract

Cerebral blood flow ensures delivery of nutrients, such as glucose, to brain sites with increased metabolic demand. However, little is known about rapid glucose dynamics at discrete locations during neuronal activation *in vivo*. Acute exposure to many substances of abuse elicits dopamine release and neuronal activation in the striatum; however, the concomitant changes in striatal glucose remain largely unknown. Recent developments have combined fast-scan cyclic voltammetry with glucose oxidase enzyme modified carbon-fiber microelectrodes to enable the measurement of glucose dynamics with subsecond temporal resolution in the mammalian brain. This work evaluates several waveforms to enable the first simultaneous detection of endogenous glucose and dopamine at single recording sites. These molecules, one electroactive and one non-electroactive, were found to fluctuate in the dorsal striatum in response to electrical stimulation of the midbrain and systemic infusion of cocaine/ raclopride. The data reveal the second-by-second dynamics of these species in a striatal microenvironment, and directly demonstrate the coupling of glucose availability with increased metabolic demand. This work provides a foundation that will enable detailed investigation of local mechanisms that regulate the coupling of cerebral blood flow with metabolic demand under normal conditions, and in animal studies of drug abuse and addiction.

Graphical Abstract

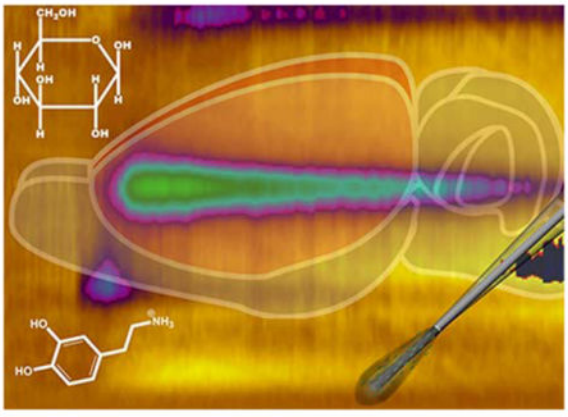

Keywords

biosensor; carbon fiber microelectrode; neuroenergetics; glucose oxidase; cocaine; fast-scan cyclic voltammetry

Introduction

Neuronal activation imposes a significant energetic demand that is fueled, at least in part, by glucose[1–3]. Cerebral blood flow (CBF) delivers glucose and other energetic resources to brain tissue in a process that is thought to be coupled to local metabolic rate[4–7]. Over 100 years ago, Roy and Sherrington reported that the vascular supply of the brain responds to local variations in functional activity[8]. Since then, many studies have described the functional recruitment of capillaries to accommodate an increased energetic demand during neuronal activation[9, 10], and brain energetics have been studied using numerous techniques. For example, imaging techniques such as positron emission tomography (PET)[11], functional magnetic resonance imaging (fMRI)[12], and high-field magnetic resonance spectroscopy (MRS)[13] have been used to monitor metabolic processes and flux in the brain with millimeter resolution. Notably, human PET studies have shown that regional cerebral oxygen consumption does not increase in response to neuronal activation to the same extent as does regional CBF[5], demonstrating a so-called uncoupling of blood flow and oxidative metabolism (for review see[10]). However, there is little direct evidence demonstrating how specific energy substrates change on a second-by-second basis in response to local neuronal activation. This is largely due to a paucity of quantitative methods with sufficient spatial and temporal resolution to selectively quantify these species on a timescale that is commensurate with that of neuronal firing. Identifying precisely how energy availability correlates with metabolic demand is a critical piece to understanding brain function.

Actions of opiates, alcohol, and major stimulants, such as cocaine, converge on the dopaminergic systems in the brain to modify synaptic activity and, ultimately, behavior[14]. The neurotransmitter dopamine (DA) modulates basal ganglia output[15] and is critically involved in cognition, sensorimotor integration, and modulation of motivated behaviors[16–23]. However, little is known about the chemical dynamics that fuel these processes, or how they are changed upon exposure to drugs of abuse. Attempts to determine how cocaine affects brain energy metabolism using PET and fMRI have provided conflicting results[24–28]. These are powerful research tools; however, they provide largely static information about glucose utilization, whereas the response to cocaine is certainly dynamic and regionally specific, confounding the issue. Furthermore, astrocytes play an important (but often overlooked) role as essential regulators of the chemical synapse. Astrocytes can deliver energetic substrates (glucose and lactate) to provide the ATP that fuels cellular function, and they also play an important role in clearing specific neurochemicals from the synaptic cleft (for review see [29,30]). Recent findings suggest that inhibiting lactate transport in the basolateral amygdala can disrupt cocaine-induced conditioned place preference, even after a cocaine priming injection, and can reduce cue-induced drug seeking in rats previously trained to self-administer cocaine[31]. Furthermore, astrocytic lactate transport in the hippocampus has been shown to contribute to long-term memory formation in rats[32], and a specific role for GluT4-

mediated glucose transport into neurons has been recently described for memory acquisition[33]. Thus, understanding how the availability of energy resources is related to neuronal activity promises to clarify some of the key molecular mechanisms that underlie normal brain function in various nuclei, as well as the changes that occur in drug abuse and addiction.

Electrochemical approaches to molecular monitoring are ideal for the detection of neurochemical dynamics *in situ* due to high spatial resolution and fast temporal response. Electrodes modified with glucose oxidase (GOx) are often coupled with amperometry for the detection of glucose *in situ*[34, 35]. Although glucose is not electroactive, GOx on the electrode surface generates glucono-1,5-lactone and hydrogen peroxide (H_2O_2) in the presence of glucose and molecular oxygen (as a cofactor). The H_2O_2 serves as the electroactive reporter molecule for glucose. However, amperometry is a non-selective technique – any substances that can oxidize at an applied potential will contribute to the current detected. Thus, it is necessary to exclude electroactive species by incorporating chemically selective polymeric layers to the electrode surface[36, 37]. It is also common to incorporate separate 'sentinel' electrodes that are identical to the GOx recording site but lack the enzyme, thus responding to all interferents but not to glucose[38, 39]. With this approach, the difference between the two recording sites is used to report on glucose concentrations. These strategies effectively eliminate interferents, but introduce confounds associated with spatial averaging, as the chemical nature of one brain site cannot be assumed to be identical to that at another site[40]. Additionally, and perhaps more importantly, they also preclude the simultaneous detection of multiple analytes, as additional species are physically filtered from the recording site, or detected but subtracted from the signal.

An alternative strategy has recently been developed by our laboratory that couples GOx enzyme modified carbon-fiber microelectrodes (GOx EME) with background-subtracted fast-scan cyclic voltammetry (FSCV) for the detection of glucose with subsecond temporal resolution in live brain tissue[41]. FSCV has been a transformative approach for quantitatively monitoring DA and other electroactive neurochemicals in brain tissue[42–45], as cyclic voltammograms serve to identify individual components of complex samples based on their electrochemical properties without requiring strategies to exclude other analytes. By combining FSCV with GOx EME, the electrochemical selectivity inherent to voltammetry enables the simultaneous detection of glucose and electroactive analytes, provided that the voltammetric response for each species is unique. The current work describes the systematic characterization and optimization of a voltammetric waveform for the reliable detection of glucose and DA at single recording sites using GOx EMEs. The optimized approach is used to simultaneously monitor both analytes in the dorsal striatum of anesthetized rats in response to electrical stimulation of the midbrain, or intravenous administration of cocaine and raclopride. The real-time measurements directly demonstrate the coupling of glucose availability with increased metabolic demand, and shed new light on the metabolic effects of augmented DA concentrations. Overall, this work provides a foundation that will enable detailed investigation of mechanisms that regulate the coupling of glucose influx with terminal activation under normal conditions, and in studies of drug abuse and addiction.

Results and Discussion

Immunohistochemistry Identifies Glucose Delivery Sites Proximal to Dopaminergic Axonal Fibers in the Striatum

Immunohistochemistry was employed to evaluate the spatial distribution of vasculature, astrocytes, and dopaminergic axonal projections in striatal brain tissue. In Figure 1, dopaminergic axonal fibers (green; visualized with rabbit anti-tyrosine hydroxylase (TH) labeled with goat anti-rabbit Alexa Fluor 488) innervate the dorsal striatum. Here, the vasculature (red; visualized with biotinylated solanum tuberosum lectin labeled with Dylight 550 conjugated streptavidin protein) can carry CBF to deliver resources into the region and remove CO_2. Energetic support can also be provided by way of astrocytes (blue; visualized with mouse anti-glial fibrillary acidic protein (GFAP) labeled with goat anti-mouse Alexa Fluor 633) which encapsulate and surround the blood vessels. These supportive cells can act independently or via networks to shuttle glucose and other energy resources to neurons[30, 46]. Figure 1 visually describes the complexity of the recording microenvironment in striatal tissue. Both the vasculature (red; lectin label) and astrocytes (blue; GFAP) are positioned to deliver glucose and other nutrients to dopaminergic fibers (green; TH label, see sites at yellow and white arrows, respectively), or to the targets of striatal DA release (i.e., medium spiny neurons (MSNs), not shown).

An Optimized Voltammetric Waveform for the Simultaneous Detection of Glucose and Dopamine

Recent developments in FSCV have enabled carbon-fiber microbiosensors to be used for the detection of rapid glucose fluctuations in the rodent brain with unprecedented temporal and spatial resolution[41]. The previous work used a triangular waveform from +0.1 V to 1.4 V with a scan rate of 400 V/s to selectively monitor glucose concentration changes *in vivo,* without requiring complicated spatial subtraction schemes or chemically selective coatings. Briefly, the oxidized form of the GOx co-factor, flavin adenine dinucleotide (FAD), is reduced as glucose is oxidized to gluconolactone, generating H_2O_2. The electrochemical oxidation of H_2O_2 at +1.4 V generates O_2, 2 protons and 2 electrons, and is measured as a change in current[47]. The resulting voltammogram identifies the H_2O_2, even in the presence of interferents, enabling it to serve as a reporter molecule for the presence of glucose. However, this voltammetric approach was optimized for sensitivity to glucose, and did not allow for the simultaneous detection of physiologically relevant concentrations of DA (below limit of detection). Figure 2 depicts the voltammetric response to DA, H_2O_2, and glucose using a bare carbon-fiber microelectrode (CFME) and a GOx EME with the previously published waveform. Representative data are depicted in color plots with corresponding background-subtracted cyclic voltammograms (CVs) shown as insets. Color plots are a simplified display of many background-subtracted CVs that enable identification of the analytes present by demonstrating the current collected at all potentials. The applied potential is plotted on the y-axis (V), time on the x-axis (sec), and current is depicted in false color (nA). Here, each color plot contains 300 voltammograms. The bare CFME (shown schematically in Figure 2A, left) detects electroactive analytes (Figure 2A, middle) such as DA (1000 nM; oxidation at ~+0.6 V indicated by asterisk) combined with a supraphysiological concentration of H_2O_2 (50 μM H_2O_2; oxidation evident at +1.2 V on the

reverse scan, indicated by triangle). However, no electrochemical signal was recorded upon delivery of 1.4 mM glucose to the CFME surface (Figure 2, right). In contrast, the GOx EME (shown schematically in Figure 2B left) was unable to detect the same concentrations of DA and H_2O_2 (Figure 2B, middle), but glucose was readily detected (Figure 2B, right). Thus, an approach to permit the simultaneous detection of physiological concentrations of both glucose and DA was sought.

A series of electrochemical waveforms was systematically characterized for the simultaneous detection of glucose and DA using the GOx EME. Triangular waveforms with holding potentials ranging from +0.1 V to −0.4 V were investigated (shown schematically in Figure 3A). GOx electrodes are most sensitive to glucose when a mildly positive holding potential is employed (+ 0.1 V); however, increasingly negative potentials were explored in an attempt to pre-concentrate positively charged DA molecules at the electrode surface and thus boost sensitivity. The switching potential was held constant, as the oxidation of H_2O_2 occurs at ~+1.4 V (but is evident at ~1.2 V on the return scan as a result of filtering)[47, 48]. Calibration curves were constructed for physiologically relevant concentrations of glucose (Figure 3B; 0.2 – 2.0 mM) and DA (Figure 3C; 250 – 1000 nM) using each waveform. Values are reported as the average ± standard error of the mean (SEM; n=5 electrodes). The linear calibration curves demonstrate that sensitivity to both analytes is dependent on holding potential. One-way ANOVA revealed that using waveforms with negative holding potentials resulted in significant changes in sensitivity to glucose and DA when compared to the previously employed +0.1 V holding potential (glucose: $F(4,20)=37.28$, $^{***}p<0.001$ and DA: $F(4,20)=70.23$, $^{***}p<0.001$). These data are listed in Table 1. Figure 3D plots the current collected in response to an injection of 2.0 mM glucose and 1000 nM DA using each of the waveforms, illustrating that sensitivity to DA improves as the holding potential decreases, but at the expense of sensitivity to glucose. DA is positively charged and can pre-concentrate at the sensing surface between voltammetric scans when negative holding potentials are employed[49]. Conversely, the isoelectric point for GOx is ~4.2, thus the protein has a net negative charge at pH 7.4. Furthermore, oxygen (the enzyme co-factor) begins to reduce at about −0.25 V. Nonetheless, a holding potential of −0.2 V affords sufficient sensitivity to both glucose and DA, and was thus selected for simultaneous measurement of these analytes.

Stability

The stability of a GOx EME coupled with this waveform was investigated over a four hour time window (Figure 4). 2 sec bolus injections of a solution containing glucose (0.8 mM) and DA (750 nM) were repeatedly introduced to the surface of the GOx EME every 15 min for four hours (typical time period of *in vivo* experiments), and stability to both analytes was assessed. Figure 4 demonstrates that the normalized current (mean ± SEM) collected in response to both analytes was stable across all time points relative to that collected in the first injection (n=4 electrodes, glucose: $F(16,48)=0.27$, $p>0.05$ and DA: $F(16,48)=0.60$, $p>0.05$). The color plots shown in Figure 4B provide representative data collected for the first and last samples analyzed at a single microbiosensor. The oxidation of DA can be identified at ~+0.6 V (asterisk), and the oxidation of H_2O_2 enzymatically generated in the

detection of glucose is depicted with a triangle. CVs that identify these analytes (inset) were extracted at the time indicated by the dashed vertical line.

Local Glucose Availability Increases in Response to Metabolic Demand

GOx EMEs were implanted in the striatum of adult, male, sprague-dawley anesthetized rats (n=4) to simultaneously record endogenous DA and glucose fluctuations at discrete recording sites. Electrical stimulation of the midbrain (60 Hz, 100–125 pulses, 200 μA) elicited striatal DA release (396 ± 29 nM). Representative data are shown in Figure 5A (left, asterisk). Electrically-elicited striatal DA release has been shown to correlate with local neural activity in subsets of MSNs[50, 51]. There is a significant energetic burden associated with the generation of action potentials, as well as in the regeneration of ionic gradients and resting potentials following synaptic events[1, 3]. Accordingly, DA release was followed by an increase in the local glucose concentration (350 ± 23 μM, triangle, n=4 animals). The voltammograms for both analytes agree with those collected *in vitro* (Figure 5A, right). Importantly, when a sample containing both glucose (triangle) and DA (asterisk) is detected *in vitro*, the electrochemical signal for glucose is generated *before* the DA signal (Figure 5B, right). H_2O_2 is enzymatically generated at the electrode surface; however, DA must diffuse through the chitosan hydrogel for detection. By contrast, a striatal glucose fluctuation evoked by electrical stimulation of the midbrain (Figure 5B, left, red) peaks 2.7 ± 0.2 sec *after* the DA release event is recorded (blue), demonstrating that glucose availability responds to meet metabolic demand. The energetic support likely fuels local MSN neuronal activation, and also provides energy to other local targets including interneurons and glial cells. The combined electrochemical detection of glucose and DA at single recording sites is a powerful tool that can be used to quantify local mechanisms that regulate glucose influx in response to terminal activation. Identifying these processes is critical to understanding brain function under control conditions as well as in response to pharmacological challenge.

Cocaine/ Raclopride Induced Fluctuations in Striatal Glucose

The acute actions of opiates, alcohol, and major stimulants such as cocaine converge on the DA circuits to modify neurochemistry and behavior[52, 53]. Certainly the administration of a drug like cocaine involves DA release in the striatum and activation of reward-associated circuits[14], but the metabolic effects of cocaine administration have proven difficult to deconvolute. There are few direct measurements of fluctuations in extracellular glucose in the brain (but see[35]), and the literature contains conflicting results [24, 26–28, 54]. Furthermore, imaging studies in human subjects are typically completed during a state of drug withdrawal or craving, as there are ethical concerns for studying an acute state, particularly with illicit substances such as cocaine. In order to directly investigate how glucose availability correlates with augmented extracellular DA concentrations at discrete recording sites in the dorsal striatum, extracellular glucose and DA dynamics were simultaneously recorded using the optimized waveform. Measurements were made before and after an intravenous (i.v.) infusion of a cocktail containing cocaine (DA transporter inhibitor) and raclopride (D2 receptor antagonist), (COC/RAC), and upon electrical stimulation. This treatment has been shown to significantly increase striatal DA release in rat striatum[55, 56].

GOx EMEs were placed in the dorsal striatum of anesthetized rats (n=4) and electrochemical data were recorded for 60 min after a systemic (i.v.) saline infusion. During this period, the midbrain was electrically stimulated after one min and every 15 min thereafter. The experimental procedure was repeated with an infusion of COC/RAC (2 mg/kg COC + 1 mg/kg RAC). At all time points, electrical stimulation evoked striatal DA release followed by local glucose influx. Representative data collected during the first electrical stimulation (lightning bolt) are shown in Figure 6, collected ~1 min after infusion of (A) saline or (B) COC/RAC. Spontaneous fluctuations in extracellular glucose concentration are evident, and glucose availability clearly increased in response to stimulation, as shown in the color plots (top panels) and in the corresponding concentration vs time traces (bottom panels). After saline administration, the amplitude of glucose influx was significantly increased by electrical stimulation, as compared to preceding spontaneous glucose signals (Figure 6C, light gray vs dark grey, two-way ANOVA: $F(3,24)=338.6$, ***$p<0.001$). This was also true after COC/RAC administration, Figure 6C, light red vs dark red, main effect of type, two-way ANOVA: $F(3,24)=7.4$, *$p<0.05$); however, statistical analysis failed to reveal any type x time interactions regardless of treatment. Additionally, glucose availability rapidly increased to meet metabolic demand in response to COC/RAC administration (Figure 6C). Both spontaneous (light gray vs light red, two-way ANOVA: $F(3,24)=36.5$ ***p<0.001), and electrically evoked (dark gray vs dark red, two-way ANOVA: $F(3,24)=5.6$ *p<0.05) glucose signals were significantly increased when compared to saline. COC/RAC-administration also elicited DA release in the dorsal striatum, consistent with prior reports of this treatment augmenting phasic DA release in the ventral striatum of anesthetized rats[55]. The amplitude of electrically evoked DA release was significantly increased at both 1 and 15 min after COC/RAC administration, as compared to saline (Figure 6D, two-way ANOVA, treatment x time: $F(3,24)=10.1$, Bonferroni post hoc comparisons; ****$p<0.0001$ and **$p<0.01$ respectively). This drug-induced effect of intravenous cocaine is in accord with the involvement of the dorsal striatum in reward and addiction[57]. Importantly, striatal DA release has been shown to differentially activate subpopulations of striatal neurons[50, 58], and cocaine is well known to elicit neural activity in the region[59, 60]. Overall, the data demonstrate that glucose influx follows electrically stimulated and pharmacologically evoked DA release, likely in response to metabolic demand within the dorsal striatum.

Extracellular glucose fuels many critical aspects of brain function, including (but not limited to) the generation of ion gradients to establish postsynaptic potentials in response to synaptic activity, and the restoration of resting membrane potential (for review see [61]). At any given moment, the extracellular glucose concentration is dependent on two opposing forces; glucose availability and metabolism. Increases in CBF and glucose consumption have *both* been correlated with an increase in metabolic demand upon neuronal activation in animal and human studies[5, 7, 62], and the physiological mechanisms that govern this have been reviewed elsewhere[61]. Wightman and colleagues have shown that electrical stimulation of the dopaminergic cell bodies in the midbrain elicits CBF in the striatum, as indicated by changes in extracellular O_2 and pH that are evident immediately following striatal DA release[63]. A combined electrochemistry/electrophysiology study has also shown that DA activates specific sub-populations of striatal targets[50]. Separate investigations conducted in rats have shown that cocaine administration consistently increases CBF[64–66] and tissue

oxygenation[66] in many brain regions, including the striatum. Furthermore, cocaine reward has been shown to increase cell firing in both the dorsal and ventral striatum of non-human primates[60]. The simultaneous measurements of glucose and DA at a single recording site reported herein are the first of their kind. They directly demonstrate that glucose influx is temporally coupled with local DA release, whether that release is evoked by electrical stimulation or COC/RAC administration (Figure 6), to help meet local energetic demand. However, it is important to note that this study investigated just one substrate in the complex neuroenergetic landscape. Lactate serves as an important alternative substrate for energy metabolism[67], and the regulation of energy for essential brain function undoubtedly involves many players including glucose, lactate, oxygen, astrocytes, neurons, and CBF. This work describes a tool that can be used to begin to study the complex interplay between these factors, and to clarify the role played by specific energy substrates and sources.

Conclusion

To date, neurochemical studies have largely focused on monitoring single analytes at a time. However, the brain is a dynamic environment of many neurochemicals working together to generate complex physiological effects. Herein, we present the first simultaneous voltammetric detection of glucose and DA at a single recording site in the rat striatum. These distinct species – one electroactive, and one non-electroactive – both rapidly fluctuate in the dorsal striatum in response to electrical stimulation of the midbrain, or COC/RAC administration. Many of the acute reinforcing effects of abused drugs, including cocaine, have been predominantly attributed increases in extracellular levels of DA in the striatum. However, the effects of striatal DA release on local glucose availability, and the physiological effects of this modulation, remain unclear. The methodology introduced herein can be used in a wide range of future studies to evaluate how striatal function is correlated with glucose availability at spatially discrete recording sites in brain nuclei associated with addiction circuits, with subsecond temporal resolution. Such measurements can help clarify the fundamental physiological response that occurs with cocaine exposure, and thus ultimately inform improved therapeutic strategies to treat cocaine abuse.

Methods

Chemicals

All chemicals were purchased and used as received from Sigma-Aldrich (St. Louis, MO), unless otherwise stated. *In vitro* electrochemical experiments were carried out in phosphate buffered saline (0.1 M PBS, containing 0.138 M NaCl and 0.0027 M KCl) at physiological pH 7.4. β-D-glucose, chitosan, and GOx from Aspergillus niger were acquired from VWR International (West Chester, PA). The chitosan (from shrimp shells) had a deacetylation percentage of ≥75% and an approximate molecular weight of 190 000–375 000 Da (practical grade). Glucose stock solution was prepared and allowed to undergo mutarotation at room temperature for at least 24 hours. All aqueous solutions were made using doubly distilled water >18 MΩ·cm (Millipore Milli-Q, Billerica, MA).

Microelectrode fabrication

Glass-insulated CFMEs were fabricated as described previously [41, 47, 68]. Briefly, a single T-650 carbon fiber (7 μm diameter, Cytec Industries, West Patterson, NJ) was aspirated into a borosilicate glass capillary (0.6 × 0.4 mm or 1.0 x 0.5 mm, A-M Systems, Carlsburg, WA) and pulled using a micropipette puller (Narishige, Tokyo, Japan) to create two sealed microelectrodes. The exposed fiber was manually cut under a microscope to a desired length, (~ 100 μm). An electrical connection was established by inserting a stainless steel wire (Squires Electronics, Inc., Cornelius, OR) coated with conductive silver paint (GC Electronics, Rockford, IL) into the back of the microelectrode.

Microbiosensor fabrication

GOx EMEs were prepared as previously described[41]. Briefly, electrodes were conditioned by the application of a voltammetric waveform of −0.4 V to +1.4 V for ~15 min at 60 Hz, and then ~5 min at 10 Hz. Thereafter, the electrodes were submersed in an aqueous solution containing 30 mg of GOx (6 mg/mL GOx in a 2% chitosan solution (pH~5.3); specific activity: 100 U/mg at 37°C). −3.0 V was applied using a DC power supply for ~30 sec to electrodeposit a chitosan hydrogel encapsulating GOx at the electrode surface. GOx EMEs were stored in PBS at 4°C prior to use.

In Vitro Experiments

All *in vitro* data were collected at room temperature in a flow-injection apparatus using commercially available HDCV software (University of North Carolina at Chapel Hill, Department of Chemistry, Electronics Facility). A micromanipulator (World Precision Instruments Inc., Sarasota, FL) was used to position the GOx EME in a custom built electrochemical cell with a continuous flow of PBS (1 mL/min) supplied by a syringe pump (New Era Pump Systems, Inc., Wantagh, NY). Two-sec bolus injections of analyte were introduced to the GOx EME surface with a 6-port HPLC valve mounted on a two-position air actuator controlled by a digital pneumonic solenoid valve (Valco Instruments Co., Inc., Houston, TX). Triangular voltammetric waveforms were applied at 400 V/s and at a frequency of 10 Hz.

In Vivo Anesthetized Experiments

All animal procedures were in accordance with the Institutional Animal Care and Use Committee (IACUC) at North Carolina State University and the National Institute for Health's Guide for the Care and Use of Laboratory Animals. Adult, male sprague-dawley rats (290 – 320 g, Charles River Laboratories, Raleigh, NC; n =4) were housed on a 12:12 hr light- dark cycle with *ad libitum* access to food and water. Rats were anesthetized with urethane (1.5 g/mL, intraperitoneal (i.p.)) and body temperature was maintained at 37°C with a heating pad throughout the duration of the experiment.

First, animals received a catheter placement into the jugular vein for sterile saline or sterile drug infusions. Once fully anesthetized, the hair was shaved away from the region targeted by the in-house surgical procedure (right side of the chest, rostral back side, and top of the head) and the skin was disinfected with alternating swabs of 70% isopropyl alcohol and betadine (3 times each). For the jugular catheter placement, a ~20 mm incision was be made

on the back and the skin was separated from the muscle tissue using hemostats in a 4 cm^2 area to accommodate the exit port of the catheter. A small incision was made in the skin 5 mm anterior to the area where the jugular vein enters the rib cage. The jugular vein was separated from the surrounding tissue using hemostats. Next, a subcutaneous burrow as made between the chest/ back incisions and the silastic end of the catheter was inserted through the incision on the back and threaded through the burrow to the area of the jugular vein. Using microscissors, a small incision was made in the jugular vein and the silastic end of the catheter as inserted 33 mm into the vein, such that the catheter nodule was flush with the incision on the vein. Sterile silk surgical thread (Ethicon, 4-0) was tied around the vein and catheter on each side of the nodule in order to secure the catheter to the vein. Then the skin on the chest/ back was secured with sutures. The catheters were flushed with 0.1 ml 70 U/ ml filtered sterile heparinized saline.

Thereafter, the stereotaxic surgical placement of electrodes was performed as described previously[41]. A GOx modified microelectrode was placed in the dorsal striatum (+ 1.2 mm anteroposterior (AP), +1.5 mm mediolateral (ML), and – 5.0 mm dorsoventral (DV), relative to bregma), and a Ag/AgCl reference electrode was inserted in the contralateral forebrain. A bipolar stimulating electrode (Plastics One, Roanoke, VA) was placed in the ventral tegmental area/ substantia nigra area of the midbrain, −5.8 mm AP, +1.0 mm ML, and −8.0 mm DV. Electrical stimulations consisted of 200 μA biphasic pulses at 60 Hz, using a pulse width of 2 ms.

Electrodes were conditioned and data were collected using HDCV software (University of North Carolina at Chapel Hill, Department of Chemistry, Electronics Facility). A jugular vein catheter was used to administer systemic (i.v., 0.6 mL) infusions of saline or drug (cocaine 2 mg/kg + raclopride 1 mg/kg, 0.3 mL) followed by 0.3 mL of saline to flush the solution through the catheter. After ~1 min, a biphasic stimulation was induced (60 Hz, 100–125 pulses, 200 μA, 2 ms pulse width), and repeated in 15 min increments for one hour.

Immunohistochemistry

Age-matched rats (n=2) were deeply anesthetized with urethane (1.5 g/mL) and transcardially perfused with 0.2 M potassium phosphate-buffered saline (KPBS), followed by 4% paraformaldehyde (PFA). All solutions were pH 7.4. Brains were removed, post-fixed for >24 hours in a 30% sucrose/ PFA solution, and cryoprotected in 30% sucrose in 0.2 M KPBS for >48 hours. Thereafter, tissue sections (40 μm) were cut with a freezing microtome (Leica) and collected in freshly prepared anti-freeze solution (30% glycerol, 30% ethylene glycol in KPBS)[69].

Immunofluorescence procedures were adapted from elsewhere[70]. Briefly, sections were washed 3 x 15 min in 0.2 M KPBS, then transferred to wells containing 3% goat serum in 0.2 M KPBS with 0.3% Triton X-100 (G-KPBS-T), which served as the blocking solution. Tissue was mildly agitated in this solution for 1 hour at room temperature. Thereafter, it was incubated for 72 hours at 4°C in a primary antibody cocktail prepared in G-KPBS-T, which contained antibodies directed against mouse glial fibrillary acidic protein (raised in mouse; 1:1000; G3893; Sigma) and tyrosine hydroxylase (raised in rabbit; 1:2500, AB5986P; Millipore). Next, the tissue was rinsed 3 x 15 min in 0.2 M KPBS. The secondary antibody

cocktail was prepared in G-KPBS-T and contained AlexaFlour 633-conjugated goat-anti-mouse immunoglobulin G (1:500; A-21052; Life Technologies) and Alexa Fluor 488-conjugated goat-anti-rabbit immunoglobulin G (1:500; A-11008; Life Technologies). Sections were incubated in the secondary cocktail for 90 min at room temperature with mild agitation. The tissue was thoroughly rinsed and placed into wells containing biotinylated solanum tuberosum lectin (2 μg/mL; B-1165; Vector Laboratories) in G-KPBS-T. The tissue was in this primary antibody solution at 4 °C for 24 hours. Tissue sections were then washed 3 x 15 min in 0.2 M KPBS and incubated for 90 min in a secondary solution of streptavidin-DyLight 550 (2 μg/mL; Cat. 84542; ThermoFisher) prepared in G-KPBS-T. Finally, sections were rinsed 3 x 15 min in 0.2 M KPBS, mounted on Superfrost plus slides (Fisher Scientific, Pittsburgh, PA), coverslipped with glycerol-based mountant (50% glycerol in 4 M sodium bicarbonate), and stored at −80°C before visualization on a confocal microscope (Leica DM5000 scope). Images were acquired, edited, and exported via Leica Application Suite AF and made into a z-stack image using ImageJ software.

Data Analysis and Statistics

HDCV Analysis software (University of North Carolina at Chapel Hill, Department of Chemistry, Electronics Facility) was used for data analysis with the multivariate statistical analysis method of principle component regression (PCR), which combines principal component analysis (PCA) with inverse least-squares regression. This approach is used to deconstruct data collected *in vivo* to reveal the relevant chemical contributors (DA, glucose, and pH) using training sets consisting of data collected *in vitro*[71]. A chemical event was defined as an event with an amplitude that exceeded three times the standard deviation of the noise. All data are shown as the mean ± standard error of the mean (SEM). Paired *t*-Test, one-way and two-way analysis of variance (ANOVA) with Bonferonni's multiple comparisons post-hoc tests were used to determine statistical differences using GraphPad Prism 5 (GraphPad Software, Inc., La Jolla, CA) when appropriate. Significance was designated as $p<0.05$.

Acknowledgments

We would like to thank Dr. James Roberts for technical assistance and assistance with manuscript preparation, and Dr. Xiaohu Xie and Dr. Jian Lu for advice with immunohistochemistry. Moreover, we would like to thank Olaf Paulson, Leif Østergaard, and Kirsten Møller for thoughtful discussion, and Deepthi Rao, Saahj Gosrani, and Anna Komsa for assistance in data collection. Funding for this work was provided by the National Science Foundation (CAREER CHE 1151264 to L.A.S.) as well as the department of Chemistry at North Carolina State University.

Abbreviations

DA	dopamine
CFME	carbon-fiber microelectrode
GOx EME	glucose oxidase enzyme modified carbon-fiber microelectrode
COC/RAC	cocktail solution containing cocaine and raclopride

References

1. Ivannikov MV, Sugimori M, Llinás RR. Calcium clearance and its energy requirements in cerebellar neurons. Cell Calcium. 2010; 47:507–513. [PubMed: 20510449]
2. Mergenthaler P, Lindauer U, Dienel GA, Meisel A. Sugar for the brain: the role of glucose in physiological and pathological brain function. Trends in Neurosciences. 2013; 36:587–597. [PubMed: 23968694]
3. Howarth C, Gleeson P, Attwell D. Updated energy budgets for neural computation in the neocortex and cerebellum. Journal of Cerebral Blood Flow and Metabolism. 2012; 32:1222–1232. [PubMed: 22434069]
4. Fellows LK, Boutelle MG. Rapid Changes in Extracellular Glucose-Levels and Blood-Flow in the Striatum of the Freely Moving Rat. Brain Research. 1993; 604:225–231. [PubMed: 8457850]
5. Fox PT, Raichle ME, Mintun MA, Dence C. Nonoxidative glucose consumption during focal physiologic neural activity. Science. 1988; 241:462–464. [PubMed: 3260686]
6. Yatsu F. Brain Work: The Coupling of Function, Metabolism and Blood Flow in the Brain. An Official Journal of the American Neurological Association and the Child Neurology Society. 1977; 1:110–110.
7. Newberg AB, Wang J, Rao H, Swanson RL, Wintering N, Karp JS, Alavi A, Greenberg JH, Detre JA. Concurrent CBF and CMRGlc changes during human brain activation by combined fMRI–PET scanning. Neuroimage. 2005; 28:500–506. [PubMed: 16084114]
8. Roy CS, Sherrington CS. On the Regulation of the Blood-supply of the Brain. The Journal of Physiology. 1890; 11:85–158.
9. Sinha AK, Klein J, Schultze P, Weiss J, Weiss HR. Cerebral Regional Capillary Perfusion and Blood-Flow After Carbon-Monoxides Exposure. Journal of Applied Physiology. 1991; 71:1196–1200. [PubMed: 1757341]
10. Paulson OB, Hasselbalch SG, Rostrup E, Knudsen GM, Pelligrino D. Cerebral blood flow response to functional activation. J Cereb Blood Flow Metab. 2010; 30:2–14. [PubMed: 19738630]
11. Raichle ME. Positron emission tomography. Annu Rev Neurosci. 1983; 6:249–267. [PubMed: 6340590]
12. Logothetis NK, Pauls J, Augath M, Trinath T, Oeltermann A. Neurophysiological investigation of the basis of the fMRI signal. Nature. 2001; 412:150–157. [PubMed: 11449264]
13. Duarte JM, Lei H, Mlynarik V, Gruetter R. The neurochemical profile quantified by in vivo 1H NMR spectroscopy. Neuroimage. 2012; 61:342–362. [PubMed: 22227137]
14. Hyman SE, Malenka RC, Nestler EJ. Neural Mechanisms of Addiction: The Role of Reward-Related Learning and Memory. Annual Review of Neuroscience. 2006; 29:565–598.
15. Graybiel AM. The basal ganglia. Current Biology. 2000; 10:R509–R511. [PubMed: 10899013]
16. Salamone JD, Correa M. The mysterious motivational functions of mesolimbic dopamine. Neuron. 2012; 76:470–485. [PubMed: 23141060]
17. Brown RG, Marsden CD. Cognitive function in Parkinson's disease: from description to theory. Trends in Neurosciences. 1990; 13:21–29. [PubMed: 1688671]
18. Covey DP, Roitman MF, Garris PA. Illicit dopamine transients: Reconciling actions of abused drugs. Trends in Neurosciences. 2014; 37:200–210. [PubMed: 24656971]
19. Haaxma CA, Helmich RCG, Borm GF, Kappelle AC, Horstink MWIM, Bloem BR. Side of symptom onset affects motor dysfunction in Parkinson's disease. Neuroscience. 2010; 170:1282–1285. [PubMed: 20723583]
20. Phillips PEM, Stuber GD, Heien M, Wightman RM, Carelli RM. Subsecond dopamine release promotes cocaine seeking. Nature. 2003; 422:614–618. [PubMed: 12687000]
21. Berridge, Kent C., TER. Parsing reward. Trends in Neuroscience. 2003; 26:507–5113.
22. Carelli MFR, Garret DS, Paul EMP, Wightman RM, Regina M. Dopamine Operates as a Subsecond Modulator of Food Seeking. The Journal of Neuroscience. 2004; 24:1265–1271. [PubMed: 14960596]

23. Malapani C, Pillon B, Dubois B, Agid Y. Impaired simultaneous cognitive task performance in Parkinson's disease: a dopamine-related dysfunction. Neurology. 1994; 44:319–326. [PubMed: 8309583]
24. Porrino DL, Friedman DP, Nader MA, Lj. Cocaine alters cerebral metabolism within the ventral striatum and limbic cortex of monkeys. The Journal of Neuroscience. 1996; 16:1230–1238. [PubMed: 8558251]
25. Hulka LM, Scheidegger M, Vonmoos M, Preller KH, Baumgartner MR, Herdener M, Seifritz E, Henning A, Quednow BB. Glutamatergic and neurometabolic alterations in chronic cocaine users measured with 1H magnetic resonance spectroscopy. Addiction Biology. 2016; 21:205–217. [PubMed: 25600822]
26. Porrino LJ, Domer FR, Crane AM, Sokoloff L. Selective alterations in cerebral metabolism within the mesocorticolimbic dopaminergic system produced by acute cocaine administration in rats. Neuropsychopharmacology. 1988; 1:109. [PubMed: 3251493]
27. London ED, Cascella NG, Wong DF, Phillips RL, Dannals RF, Links JM, Herning R, Grayson R, Jaffe JH, Wagner HN. Cocaine-Induced Reduction of Glucose-Utlization in Human Brain- A Study Using Positron Emission Tomography and [Flourine-18]-Fluorodeoxyglucose. Archives of General Psychiatry. 1990; 47:567–574. [PubMed: 2350209]
28. Thomas WL, Cooke ES, Hammer RP. Cocaine-induced sensitization of metabolic activity in extrapyramidal circuits involves prior dopamine D1-like receptor stimulation. Journal of Pharmacology and Experimental Therapeutics. 1996; 278:347–353. [PubMed: 8764369]
29. Dienel GA. Brain lactate metabolism: the discoveries and the controversies. J Cereb Blood Flow Metab. 2012; 32:1107–1138. [PubMed: 22186669]
30. Magistretti, Pierre J., Allaman, I. A Cellular Perspective on Brain Energy Metabolism and Functional Imaging. Neuron. 2015; 86:883–901. [PubMed: 25996133]
31. Zhang Y, Xue Y, Meng S, Luo Y, Liang J, Li J, Ai S, Sun C, Shen H, Zhu W, Wu P, Lu L, Shi J. Inhibition of Lactate Transport Erases Drug Memory and Prevents Drug Relapse. Biol Psychiatry. 2016; 79:928–939. [PubMed: 26293178]
32. Suzuki A, Stern SA, Bozdagi O, Huntley GW, Walker RH, Magistretti PJ, Alberini CM. Astrocyte-neuron lactate transport is required for long-term memory formation. Cell. 2011; 144:810–823. [PubMed: 21376239]
33. McNay EC, McCarty RC, Gold PE. Fluctuations in Brain Glucose Concentration during Behavioral Testing: Dissociations between Brain Areas and between Brain and Blood. Neurobiol Learn Mem. 2001; 75:325–337. [PubMed: 11300738]
34. Hu Y, Wilson GS. Rapid Changes in Local Extracellular Rat Brain Glucose Observed with an In Vivo Glucose Sensor. Journal of Neurochemistry. 1997; 68:1745–1752. [PubMed: 9084449]
35. Kiyatkin EA, Lenoir M. Rapid fluctuations in extracellular brain glucose levels induced by natural arousing stimuli and intravenous cocaine: fueling the brain during neural activation. Journal of Neurophysiology. 2012; 108:1669–1684. [PubMed: 22723672]
36. Dale N, Hatz S, Tian F, Llaudet E. Listening to the brain: microelectrode biosensors for neurochemicals. Trends in Biotechnology. 2005; 23:420–428. [PubMed: 15950302]
37. Wang J. Electrochemical Glucose Biosensors. Chemical Reviews. 2008; 108:814–825. [PubMed: 18154363]
38. Wei WJ, Song YL, Fan XY, Zhang S, Wang L, Xu SW, Wang MX, Cai XX. Simultaneous recording of brain extracellular glucose, spike and local field potential in real time using an implantable microelectrode array with nano-materials. Nanotechnology. 2016; 27:114001–114006. [PubMed: 26871752]
39. Lourenço CF, Ledo A, Laranjinha J, Gerhardt GA, Barbosa RM. Microelectrode array biosensor for high-resolution measurements of extracellular glucose in the brain. Sensors and Actuators B: Chemical. 2016; 237:298–307.
40. Wightman RM, Heien MLAV, Wassum KM, Sombers LA, Aragona BJ, Khan AS, Ariansen JL, Cheer JF, Phillips PEM, Carelli RM. Dopamine release is heterogeneous within microenvironments of the rat nucleus accumbens. European Journal of Neuroscience. 2007; 26:2046–2054. [PubMed: 17868375]

41. Lugo-Morales LZ, Loziuk PL, Corder AK, Toups JV, Roberts JG, McCaffrey KA, Sombers LA. Enzyme-Modified Carbon-Fiber Microelectrode for the Quantification of Dynamic Fluctuations of Nonelectroactive Analytes Using Fast-Scan Cyclic Voltammetry. Analytical Chemistry. 2013; 85:8780–8786. [PubMed: 23919631]
42. Nguyen MD, Venton BJ. Fast-scan Cyclic Voltammetry for the Characterization of Rapid Adenosine Release. Computational and Structural Biotechnology Journal. 2015; 13:47–54. [PubMed: 26900429]
43. Roberts JG, Hamilton KL, Sombers LA. Comparison of electrode materials for the detection of rapid hydrogen peroxide fluctuations using background-subtracted fast scan cyclic voltammetry. Analyst. 2011; 136:3550–3556. [PubMed: 21727955]
44. Hashemi P, Dankoski EC, Lama R, Wood KM, Takmakov P, Wightman RM. Brain dopamine and serotonin differ in regulation and its consequences. Proceedings of the National Academy of Sciences of the United States of America. 2012; 109:11510–11515. [PubMed: 22778401]
45. Park J, Takmakov P, Wightman RM. In vivo comparison of norepinephrine and dopamine release in rat brain by simultaneous measurements with fast-scan cyclic voltammetry. Journal of Neurochemistry. 2011; 119:932–944. [PubMed: 21933188]
46. Harris JJ, Jolivet R, Attwell D. Synaptic Energy Use and Supply. Neuron. 2012; 75:762–777. [PubMed: 22958818]
47. Sanford AL, Morton SW, Whitehouse KL, Oara HM, Lugo-Morales LZ, Roberts JG, Sombers LA. Voltammetric Detection of Hydrogen Peroxide at Carbon Fiber Microelectrodes. Analytical Chemistry. 2010; 82:5205–5210. [PubMed: 20503997]
48. Roberts JG, Voinov MA, Schmidt AC, Smirnova TI, Sombers LA. The Hydroxyl Radical is a Critical Intermediate in the Voltammetric Detection of Hydrogen Peroxide. JOURNAL OF THE AMERICAN CHEMICAL SOCIETY. 2016; 138:2516–2519. [PubMed: 26840154]
49. Heien M, Phillips PEM, Stuber GD, Seipel AT, Wightman RM. Overoxidation of carbon-fiber microelectrodes enhances dopamine adsorption and increases sensitivity. Analyst. 2003; 128:1413–1419. [PubMed: 14737224]
50. Owesson-White C, Belle AM, Herr NR, Peele JL, Gowrishankar P, Carelli RM, Wightman XM. Cue-Evoked Dopamine Release Rapidly Modulates D2 Neurons in the Nucleus Accumbens During Motivated Behavior. Journal of Neuroscience. 2016; 36:6011–6021. [PubMed: 27251622]
51. Cheer JF, Aragona BJ, Heien MLAV, Seipel AT, Carelli RM, Wightman RM. Coordinated Accumbal Dopamine Release and Neural Activity Drive Goal-Directed Behavior. Neuron. 2007; 54:237–244. [PubMed: 17442245]
52. Nestler EJ. Is there a common molecular pathway for addiction? Nature Neuroscience. 2005; 8:1445–1449. [PubMed: 16251986]
53. Wise RA. Dopamine, learning and motivation. Nature Reviews Neuroscience. 2004; 5:483–494. [PubMed: 15152198]
54. Porrino LJ, Lyons D, Miller MD, Smith HR, Friedman DP, Daunais JB, Nader MA. Metabolic Mapping of the Effects of Cocaine during the Initial Phases of Self-Administration in the Nonhuman Primate. The Journal of Neuroscience. 2002; 22:7687–7694. [PubMed: 12196592]
55. McCutcheon JE, Cone JJ, Sinon CG, Fortin SM, Kantak PA, Witten IB, Deisseroth K, Stuber GD, Roitman MF. Optical suppression of drug-evoked phasic dopamine release. Frontiers in Neural Circuits. 2014; 8:1–8. [PubMed: 24478635]
56. Park J, Aragona BJ, Kile BM, Carelli RM, Wightman RM. In Vivo Voltammetric Monitoring of Catecholamine Release in Subterritories of the Nucleus Accumbens Shell. Neuroscience. 2010; 169:132–142. [PubMed: 20451589]
57. Wise RA. Roles for nigrostriatal—not just mesocorticolimbic—dopamine in reward and addiction. Trends in Neurosciences. 2009; 32:517–524. [PubMed: 19758714]
58. White IM, Doubles L, Rebec GV. Cocaine-induced activation of striatal neurons during focused stereotypy in rats. Brain Research. 1998; 810:146–152. [PubMed: 9813293]
59. Carelli RM. Activation of accumbens cell firing by stimuli associated with cocaine delivery during self-administration. Synapse. 2000; 35:238–242. [PubMed: 10657032]

60. Opris I, Hampson RE, Deadwyler SA. The encoding of cocaine vs. natural rewards in the striatum of nonhuman primates: categories with different activations. Neuroscience. 2009; 163:40–54. [PubMed: 19501630]

61. Paulson OB, Hasselbalch SG, Rostrup E, Knudsen GM, Pelligrino D. Cerebral blood flow response to functional activation. J Cereb Blood Flow Metab. 2009; 30:2–14. [PubMed: 19738630]

62. Madsen PL, Hasselbalch SG, Hagemann LP, Olsen KS, Bulow J, Holm S, Wildschiodtz G, Paulson OB, Lassen NA. Persistent Resetting of the Cerebral Oxygen Glucose Uptake Ratio by Brain Activation: Evidence Obtained with the Kety-Schmidt Technique. Journal of Cerebral Blood Flow & Metabolism. 1995; 15:485–491. [PubMed: 7714007]

63. Venton BJ, Michael DJ, Wightman RM. Correlation of local changes in extracellular oxygen and pH that accompany dopaminergic terminal activity in the rat caudate–putamen. J Neurochem. 2003; 84:373–381. [PubMed: 12558999]

64. Schmidt KF, Febo M, Shen Q, Luo F, Sicard KM, Ferris CF, Stein EA, Duong TQ. Hemodynamic and metabolic changes induced by cocaine in anesthetized rat observed with multimodal functional MRI. Psychopharmacology. 2006; 185:479–486. [PubMed: 16550388]

65. Stein EA, Fuller SA. Cocaine's time action profile on regional cerebral blood flow in the rat. Brain Research. 1993; 626:117–126. [PubMed: 8281422]

66. Ceolin L, Schwarz AJ, Gozzi A, Reese T, Bifone A. Effects of cocaine on blood flow and oxygen metabolism in the rat brain: implications for phMRI. Magnetic Resonance Imaging. 2007; 25:795–800. [PubMed: 17442519]

67. Hu Y, Wilson GS. A temporary local energy pool coupled to neuronal activity: fluctuations of extracellular lactate levels in rat brain monitored with rapid-response enzyme-based sensor. J Neurochem. 1997; 69:1484–1490. [PubMed: 9326277]

68. Roberts, J., Lugo-Morales, L., Loziuk, P., Sombers, L. Real-Time Chemical Measurements of Dopamine Release in the Brain. In: Kabbani, N., editor. Dopamine. Humana Press; 2013. p. 275-294.

69. Hoffman GE, Le WW. Just cool it! Cryoprotectant anti-freeze in immunocytochemistry and in situ hybridization. Peptides. 2004; 25:425–431. [PubMed: 15134865]

70. Bucher ES, Fox ME, Kim L, Kirkpatrick DC, Rodeberg NT, Belle AM, Wightman RM. Medullary norepinephrine neurons modulate local oxygen concentrations in the bed nucleus of the stria terminalis. J Cereb Blood Flow Metab. 2014; 34:1128–1137. [PubMed: 24714037]

71. Keithley RB, Heien ML, Wightman RM. Multivariate concentration determination using principal component regression with residual analysis. Trends in Analytical Chemistry. 2009; 28:1127–1136. [PubMed: 20160977]

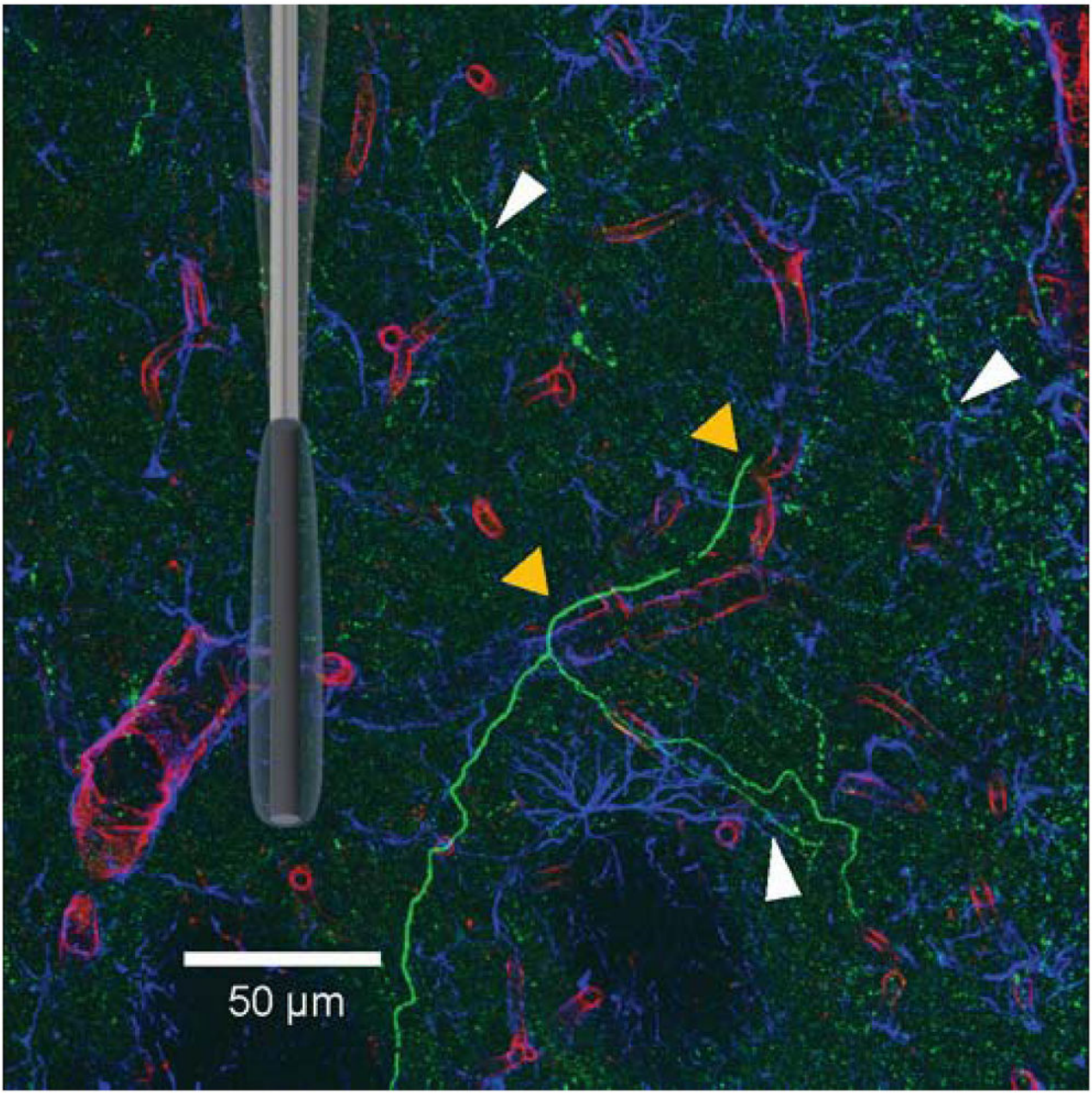

Figure 1.

Triple-Fluorescence Labeling in the Rat Dorsal Striatum. Confocal laser image (275 x 275 µm) taken from a 40 µm-thick tissue slice. Sites where dopaminergic axonal fibers (green; TH label) interact with blood vessels (red; lectin label) and/ or astrocytes (blue; GFAP label) are indicated by the triangles (yellow and white, respectively). A randomly oriented and scaled schematic of a GOx EME is superimposed to demonstrate its relative size in this environment. Scale bar is 50 µm.

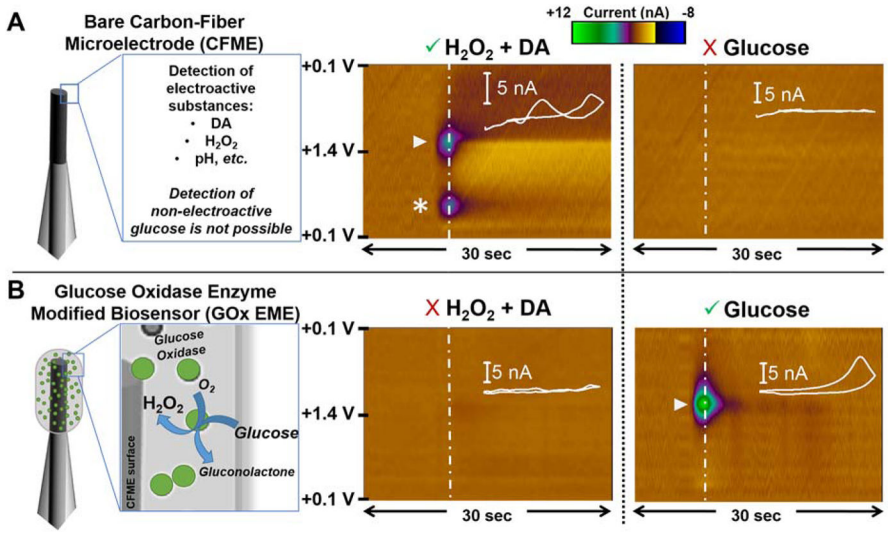

Figure 2.

Voltammetric Response of Carbon-Fiber Microsensors to Glucose, Dopamine and H_2O_2. (A) Left: Schematic representation of a bare CFME. Representative color plots depict current collected in response to the same solutions using a voltammetric waveform from +0.1 V to +1.4 V[41]. A mixture of 1000 nM DA (asterisk) and 50 μM H_2O_2 (triangle) is detected (middle), but the detection of non-electroactive glucose (0.8 mM) is precluded (right). (B) Left: Schematic of the GOx EME. Right: Representative color plots demonstrate the detection of glucose (triangle, indicated by the oxidation of enzymatically generated H_2O_2). However, there is insufficient sensitivity for the detection of physiologically relevant concentrations of H_2O_2 and DA (middle panel).

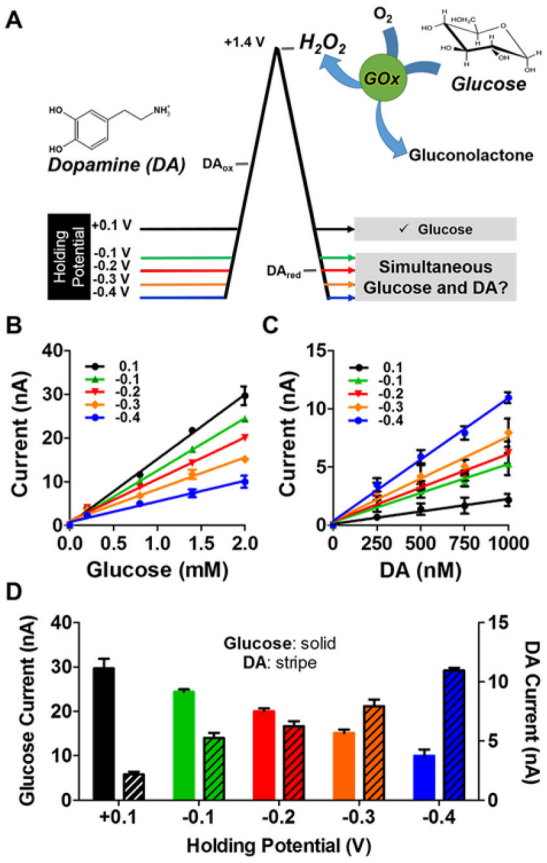

Figure 3.

Systematic Characterization of Holding Potential. (A) Investigation of a series of waveforms for the simultaneous voltammetric detection of glucose and DA with a GOx EME. (B) Glucose (0.2–2.0 mM) and (C) DA (250–1000 nM) calibration plots collected with the waveforms shown in (A). (D) The current collected in response to a sample containing 2.0 mM glucose and 1000 nM DA (note respective scales on left and right y-axes) is dependent on the holding potential applied between voltammetric scans. A −0.2 V holding potential provides a compromise that enables adequate detection of both analytes. One-way ANOVA analysis demonstrated all holding potentials were significantly different than the previously employed +0.1 V holding potential (glucose: $F(4,20)=37.28$, ***$p<0.001$ and DA: $F(4,20)=70.23$, ***$p<0.001$).

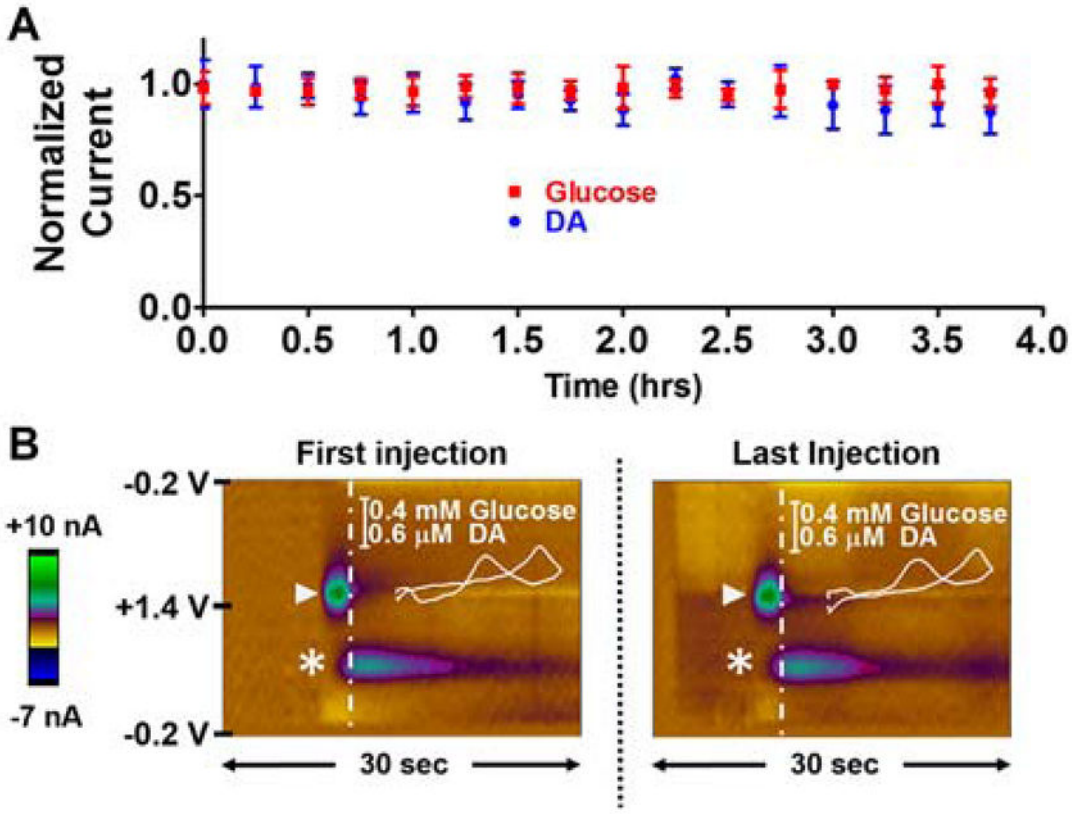

Figure 4.

Microbiosensor Stability. (A) Normalized current collected in response to repeated bolus injections of a solution containing glucose (0.8 mM) and DA (750 nM). The peak current remained stable for glucose ($F(16,48)=0.27$, $p>0.05$) and DA ($F(16,48)=0.60$, $p>0.05$) over 4 hours. (B) Representative color plots for the first (left) vs last (right) injection. Analyte identification (glucose: triangle, DA: asterisk) is achieved using CVs extracted from the color plot at the time indicated by the vertical dashed line (inset).

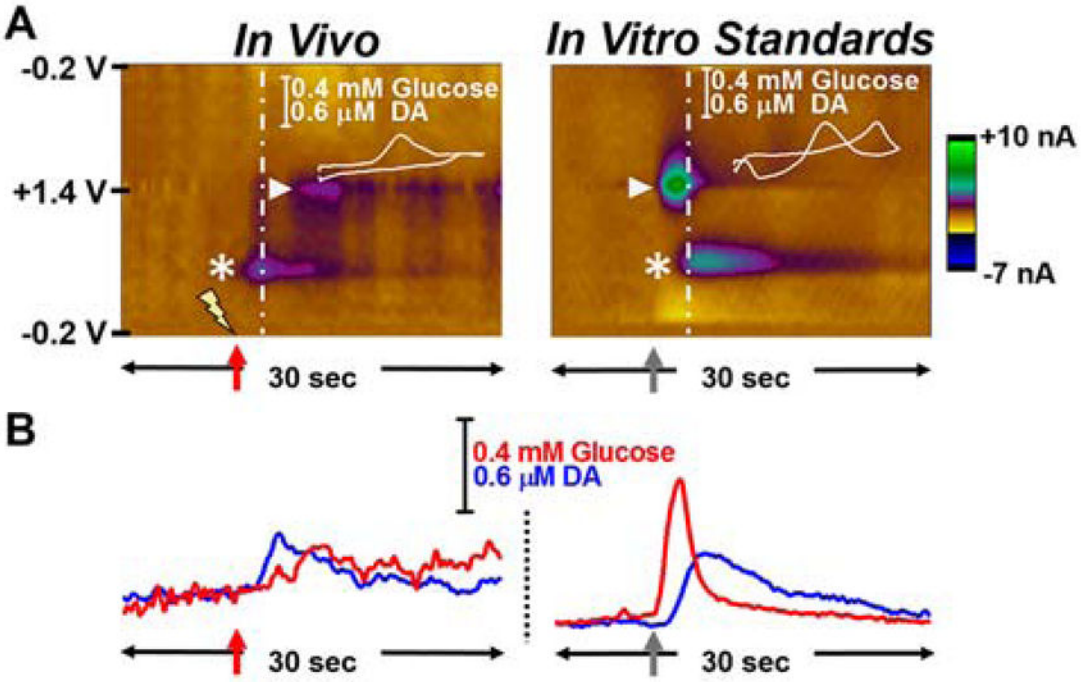

Figure 5.

Comparison of *in vivo* vs *in vitro* chemical dynamics. Representative data in the form of (A) color and (B) concentration vs time plots provide a visual comparison of the dynamics of glucose and DA detection. Left: When recording in the striatum of the anesthetized rat, electrical stimulation of the midbrain (60 Hz, 100–125 pulses, 200 μA, indicated by lightning bolt and red arrow) elicited DA release (asterisk) followed by an increase in extracellular glucose (triangle). Right: Glucose is detected prior to DA when a bolus of these standards is detected *in vitro* (sample delivery indicated by gray arrow). These data demonstrate that glucose availability responds to meet metabolic demand in the striatum following electrical stimulation of the midbrain.

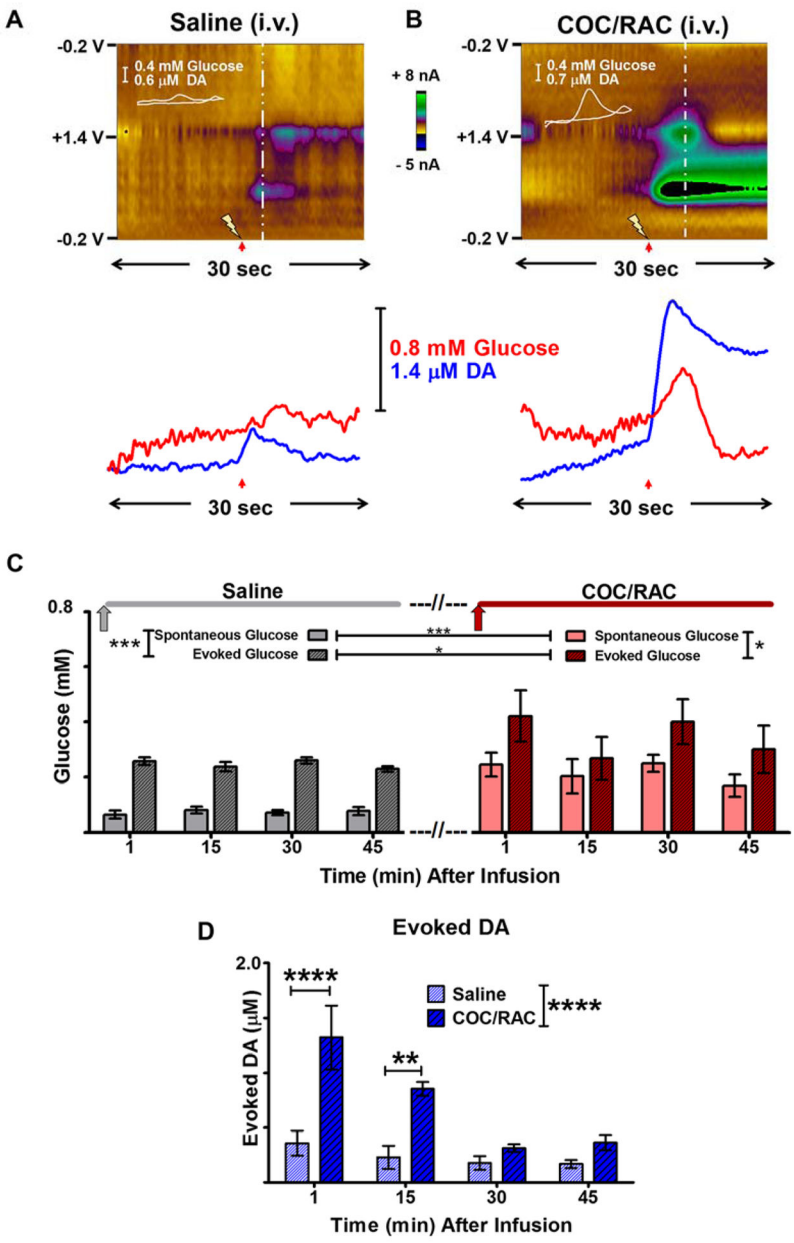

Figure 6.

Glucose availability is coupled with metabolic demand. Top: Representative color plots collected after i.v. infusion of (A) saline or (B) COC/RAC. The time of midbrain stimulation (60 Hz, 100–125 biphasic pulses, 200 µA) is indicated by the lightning bolt and red arrow. Bottom: Electrical stimulation evoked striatal DA release (blue) followed by local glucose influx (red), as evident in the concentration vs time profiles. (C) After saline infusion, electrical stimulation of the midbrain increased glucose influx to the recording site (dark gray v light gray), at all time points (***p<0.001). This trend held after treatment with COC/RAC (light red vs dark red, *p <0.05). COC/RAC treatment augmented spontaneous glucose influx to the sampling site (light gray vs light red, ***p<0.001). Electrical stimulation further increased extracellular glucose concentrations, as compared to

electrically evoked glucose influx after saline administration (dark gray vs dark red, *p<0.05). (D) COC/RAC treatment significantly increased electrically evoked DA release at the 1 and 15 min time points when compared to saline (Bonferroni post hoc test, ****p<0.001, **p<0.01 respectively).

Table 1

Sensitivity to Glucose and DA. Data were collected using a series of triangular waveforms coupled to a GOx EME, and are plotted in Figures 2B and C.

Holding Potential	Glucose Sensitivity (nA/mM)	Glucose r^2	Glucose % Difference vs. +0.1 V	DA Sensitivity (nA/μM)	DA r^2	DA % Difference vs. +0.1 V
+0.1 V	14.8 ± 0.4	0.99	0	2.1 ± 0.2	0.98	0
−0.1 V	12.0 ± 0.3	0.99	−18.8**	5.0 ± 0.4	0.98	138.1*
−0.2 V	9.6 ± 0.5	0.99	−35.1***	5.8 ± 0.6	0.97	176.2**
−0.3 V	7.3 ± 0.6	0.98	−50.7***	7.2 ± 0.9	0.96	242.9***
−0.4 V	4.7 ± 0.4	0.98	−68.2***	10.6 ± 0.5	0.99	404.8***

Bonferroni post hoc comparisons revealed significant differences compared to a +0.1 V holding potential (*p<0.05, **p<0.01, *** p<0.001).